

See discussions, stats, and author profiles for this publication at: <https://www.researchgate.net/publication/275350002>

Stable high-performance hybrid perovskite solar cells with ultrathin polythiophene as hole-transporting layer

ARTICLE *in* NANO RESEARCH · APRIL 2015

Impact Factor: 7.01 · DOI: 10.1007/s12274-015-0755-5

CITATIONS

4

READS

77

8 AUTHORS, INCLUDING:



Weibo Yan

Peking University

23 PUBLICATIONS 129 CITATIONS

[SEE PROFILE](#)



Yunlong Li

Peking University

10 PUBLICATIONS 40 CITATIONS

[SEE PROFILE](#)



Shufeng Wang

Peking University

120 PUBLICATIONS 1,550 CITATIONS

[SEE PROFILE](#)



Zuqiang Bian

Peking University

81 PUBLICATIONS 1,405 CITATIONS

[SEE PROFILE](#)

Stable high-performance hybrid perovskite solar cells with ultrathin polythiophene as hole-transporting layer

Weibo Yan¹, Yunlong Li¹, Yu Li², Senyun Ye¹, Zhiwei Liu¹, Shufeng Wang² (✉), Zuqiang Bian¹ (✉), Chunhui Huang¹ (✉)

¹ State Key Laboratory of Rare Earth Materials Chemistry and Applications, College of Chemistry and Molecular Engineering, Peking University, Beijing, 100871, China

² State Key Laboratory for Mesoscopic Physics, Department of Physics, Peking University, Beijing 100871, China

Received: 16 January 2015

Revised: 16 February 2015

Accepted: 17 February 2015

© Tsinghua University Press
and Springer-Verlag Berlin
Heidelberg 2015

KEYWORDS

perovskite solar cells,
polythiophene,
hole-transporting layer,
electrochemical
polymerization

ABSTRACT

Ultrathin polythiophene films prepared via electrochemical polymerization is successfully used as the hole-transporting material, substituting conventional HTM-PEDOT:PSS, in planar p-i-n $\text{CH}_3\text{NH}_3\text{PbI}_3$ perovskite-based solar cells, affording a series of ITO/polythiophene/ $\text{CH}_3\text{NH}_3\text{PbI}_3/\text{C}_{60}/\text{BCP}/\text{Ag}$ devices. The ultrathin polythiophene film possesses good transmittance, high conductivity, a smooth surface, high wettability, compatibility with PbI_2 DMF solution, and an energy level matching that of the $\text{CH}_3\text{NH}_3\text{PbI}_3$ perovskite material. A promising power conversion efficiency of about 15.4%, featuring a high fill factor of 0.774, open voltage of 0.99 V, and short-circuit current density of $20.3 \text{ mA}\cdot\text{cm}^{-2}$ is obtained. The overall performance of the devices is superior to that of cells using PEDOT:PSS. The differences of solar cells with different hole-transfer materials in charge recombination, charge transport and transfer, and device stability are further investigated and demonstrate that polythiophene is a more effective and promising hole-transporting material. This work provides a simple, prompt, controllable, and economic approach for the preparation of an effective hole-transporting material, which undoubtedly offers an alternative method in the future industrial production of perovskite solar cells.

In the past few years, $\text{CH}_3\text{NH}_3\text{PbX}_3$ ($\text{X} = \text{Cl}, \text{Br}, \text{I}$) perovskite has been proven to be a remarkable light harvester and hole conductor in hybrid perovskite solar cells. [1–4] Optimized perovskite solar cells have reached up to 19.3% efficiency by Prof. Yang's group, which confirms the commercial prospects of this variety of solar cell. [4] Therefore, the design of new device

structures [1, 5, 6] and the exploration of new hole [7–10] and electron-transporting [1, 11–13] layers is very important to reduce the cost of practical production, while maintaining the stable and excellent performance of these solar cells.

In perovskite solar cells, several conducting polymers such as P3HT, [14] PEDOT:PSS, [5] poly-(triarylamine),

Address correspondence to Zuqiang Bian, email bianzq@pku.edu.cn; Shufeng Wang, email wangsf@pku.edu.cn



[15] and graphene-based materials, [9, 10] as well as some small molecules such as spiro-OMeTAD, [1] pyrene-core arylamine derivatives, [16] and CuI [8] have been used as hole-transporting materials (HTM) in perovskite-based solar cells. Spiro-OMeTAD has been demonstrated to be an effective small-molecule HTM for perovskite solar cells. However, the extensive synthetic process for spiro-OMeTAD limits its use in large-scale operations. In planar p-i-n perovskite-based solar cells, conventional PEDOT:PSS was successfully used as an HTM, but it seriously deteriorated the stability of the perovskite due to its high hygroscopicity, which led to the decomposition of the perovskite. [5] In general, the high cost of HTM, its low performance in the device, or both hinder the advancement of cost-effective and practical perovskite-based solar cells.

Herein, we report on the photovoltaic properties of HTM/CH₃NH₃PbI₃/C₆₀ solar cells using an optimized ultrathin polythiophene (PT) film as the HTM, with PEDOT:PSS as a reference. The differences in the devices' charge recombination, charge transport and transfer, light-to-current conversion performance, and stability were further investigated, to understand why PT is a more effective and promising HTM than PEDOT:PSS.

The room-temperature out-of-plane resistance of

the PT films, measured using a two-probe method, was about 15 Ω, which was lower than that of the PEDOT:PSS films (see Fig. S2). The work function of PT was -5.18 eV, measured by UPS. This approaches the energy of the highest occupied molecular orbital (HOMO, -5.4 eV) of the CH₃NH₃PbI₃ perovskite more closely than that (-5.09 eV) of PEDOT:PSS, as shown in Fig. S3. The closeness of PT's HOMO level to that of CH₃NH₃PbI₃ perovskite facilitates hole transfer to the ITO electrode through the PT layer. The PT films were almost transparent to electromagnetic radiation below 400 nm and above 600 nm, and the transmittance of a 5-nm-thick PT film approached 94% at its absorption maximum of 520 nm (see Fig. 1(a)). This high transmittance would greatly reduce the adverse effect of the short-circuit current (J_{sc}) in planar p-i-n solar cell devices. The vibration peaks at 1,330 and 640 cm⁻¹ for PT (see Fig. S2(c)) are characteristic for doped PT. [17] Further XPS characterization of PT (see Fig. S2(d)) was conducted to estimate the extent of doping; from the C/F atom ratio (1:0.055) of PT, one BF₄⁻ group was calculated to exist on average for every 18 thiophene units.

Thin PT film obtained via electrochemical polymerization was extremely smooth. Its dimethylformamide (DMF) contact angles of L = 2.6° and R = 2.6°

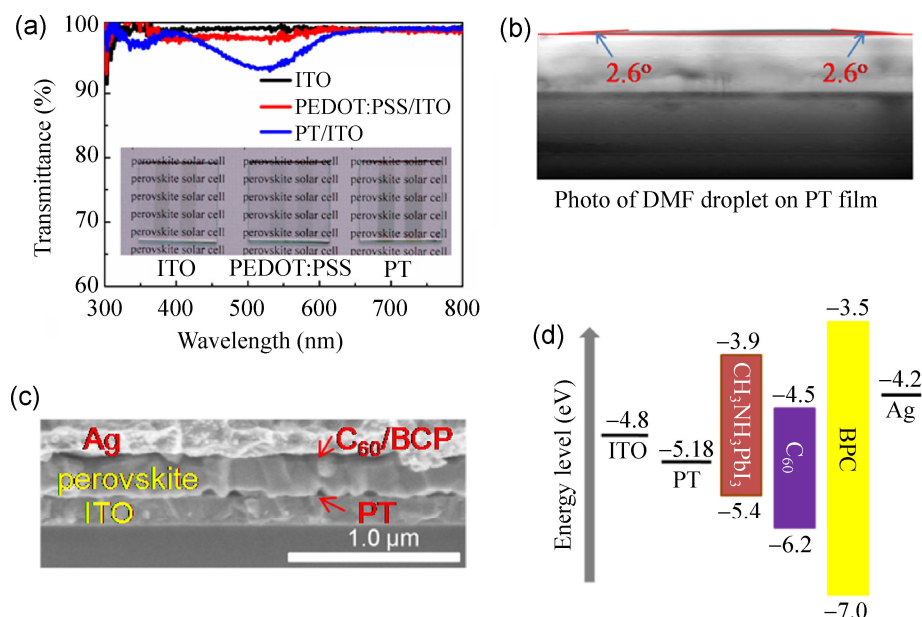


Figure 1 (a) Transmittance spectra of PEDOT:PSS/ITO and PT/ITO glass with ITO glass as reference (100%); (b) Dimethylformamide (DMF) contact angle of PT film; (c) Cross-sectional SEM image of the planar perovskite solar cell using PT as the HTM; (d) The relative energy level diagram of the perovskite solar cell.

show the high wettability and compatibility between the PT film surface and the DMF solution (see Fig. 1(b)). This shows that a PbI_2 solution in DMF spin-coated onto PT film could form a high-quality PbI_2 film. Following this with immersion of the substrate in a $\text{CH}_3\text{NH}_3\text{I}$ solution of 2-propanol creates the perovskite phase (see Fig. S3). SEM images (see Fig. S4) show the good crystallinity of the obtained perovskite, and the grazing-angle X-ray diffraction (GAXRD) patterns of $\text{CH}_3\text{NH}_3\text{PbI}_3$ perovskite agree well with previously published results. [5, 18] Furthermore, we also investigated $\text{CH}_3\text{NH}_3\text{PbI}_3$ perovskite films with different thickness obtained from 0.8–1.1 M PbI_2 solution. These showed no change in diffraction peak location or relative intensity, which indicated the reliability of this two-step method to produce $\text{CH}_3\text{NH}_3\text{PbI}_3$ perovskite, as well as its insensitivity to concentration changes (see Fig. S5). The investigation also confirms the reliability of optimization based on the change in thickness of the $\text{CH}_3\text{NH}_3\text{PbI}_3$ perovskite layer in the devices.

Planar perovskite solar cells featuring a structure of ITO/PT/ $\text{CH}_3\text{NH}_3\text{PbI}_3/\text{C}_{60}/\text{BCP/Ag}$ were fabricated using the previously described process. [18] To probe the effect of the perovskite layer thickness on the device performance, devices with $\text{CH}_3\text{NH}_3\text{PbI}_3$ (180–270 nm)/ C_{60} (40 nm)/BCP (10 nm) construction were firstly prepared by varying the concentration of PbI_2 to 0.8, 0.9, 1.0, and 1.1 M to control the thickness of the deposited PbI_2 films (95, 110, 126, and 140 nm, respectively) and obtain $\text{CH}_3\text{NH}_3\text{PbI}_3$ perovskite films with thicknesses of approximately 180, 210, 245, and 270 nm, respectively. As the thickness of the $\text{CH}_3\text{NH}_3\text{PbI}_3$ perovskite layer increased, more radiation light was absorbed and the J_{sc} of the devices increased at first. When the films became too thick, the J_{sc} decreased, probably due to the increased carrier recombination rate. Furthermore, the fill factor (FF) stabilized above 0.70, simultaneous with a small change of the V_{oc} from 0.94 to 1.00 V (see Fig. S6).

With a constant perovskite layer thickness of about 245 nm, the devices were further optimized by depositing different thickness of the C_{60} layer (30, 40, and 50 nm) and the BCP layer (5, 10, and 15 nm) (see Fig. S6, Table S2, and S3). As the thickness of C_{60} increased to 50 nm, the FF increased up to 0.81, while the J_{sc} decreased and V_{oc} remained nearly constant.

Changing the thickness of BCP had little effect on the device's FF, but when its thickness increased up to 15 nm, the J_{sc} decreased greatly, due to the increased resistance of the BCP layer. After optimization, the devices with the highest conversion efficiency of 15.4% were obtained with V_{oc} of 0.99 V, J_{sc} of 20.3 mA cm^{-2} , and FF of 0.774 in a structure of ITO/PT (5 nm)/ $\text{CH}_3\text{NH}_3\text{PbI}_3$ (245 nm)/ C_{60} (40 nm)/BCP (10 nm)/Ag (100 nm) (see Fig. 2(a)). Using the optimal architecture of $\text{CH}_3\text{NH}_3\text{PbI}_3$ (245 nm)/ C_{60} (40 nm)/BCP (10 nm), the device's performance with PEDOT:PSS as HTM layer was investigated in comparison. As seen in Fig. 2(b), lower V_{oc} of about 0.93 V, FF of 70%, and J_{sc} of 18.5 mA cm^{-2} are obtained.

As shown in Fig. 2(c), the incident-photon-to-current efficiency (IPCE) spectrum for the device using ultrathin PT as HTM shows a response in the region from the UV-visible to near infrared range (300–800 nm) with no obviously lower IPCE from 400 to 600 nm observed, which indicates that the ultrathin PT layer absorbs little of the incident light and thus has negligible effects on the J_{sc} . The calculated J_{sc} integrated from the IPCE is 19.5 mA cm^{-2} , around 5% lower than the J_{sc} of about 20.3 mA cm^{-2} obtained from $J-V$ measurement. A relatively lower IPCE value is obtained from the PEDOT:PSS-based device, which confirms that $\text{CH}_3\text{NH}_3\text{PbI}_3$ perovskite solar cells with PT HTM show better performance than those with PEDOT:PSS.

Time-resolved photoluminescence (PL) behavior was characterized to probe the charge transfer occurring at the interface between the perovskite and HTM layers. Detailed information regarding the preparation, measurement, and fitting methodology can be found in the experimental section. The PL lifetime of the samples was fitted with a bi-exponential decay function containing both fast and slow decay processes. The fast decay process was considered to result from the quenching of free carriers in the perovskite domain through their transport to PT or PEDOT:PSS, and the slow decay process from radiative decay. Figure 2(d) displays the PL decay and the related parameters are summarized in Table S4. For pristine thin-film perovskite, the decay lifetime is 17.3 ns, consistent with previous reports, [19] indicating the good quality of the obtained $\text{CH}_3\text{NH}_3\text{PbI}_3$ perovskite. With the existence of the quenching HTM layer atop the perovskite, for

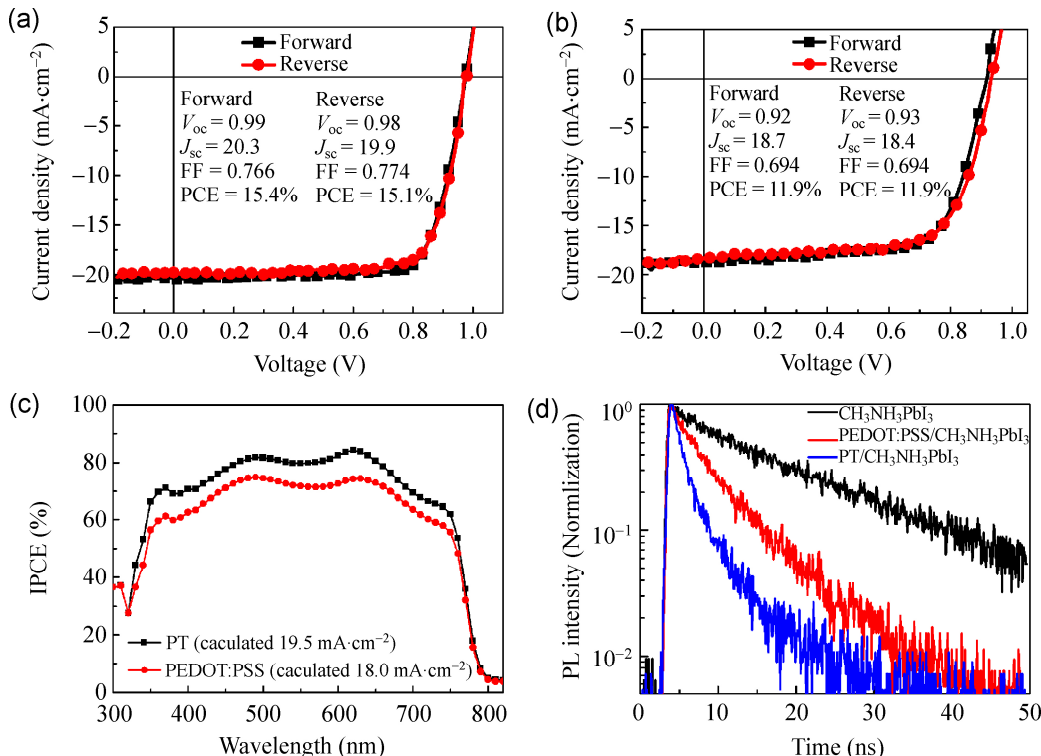


Figure 2 Current-density/voltage curves of the best-performing planar heterojunction HTM/perovskite/ C_{60} solar cells (a) using PT as HTM; (b) using PEDOT:PSS as HTM; (c) IPCE spectrum of the HTM/perovskite/ C_{60} device; (d) Time-resolved photoluminescence behavior of $\text{CH}_3\text{NH}_3\text{PbI}_3$, PEDOT:PSS/ $\text{CH}_3\text{NH}_3\text{PbI}_3$, and PT/ $\text{CH}_3\text{NH}_3\text{PbI}_3$.

perovskite/PT, the fast decay lifetime is 1.17 ns and the slow decay lifetime is 4.81 ns with weight fractions of 83.2% and 16.8%, respectively, indicating that the charge transfer mechanism dominates PL decay. For perovskite/PEDOT:PSS, the fast decay lifetime increases to 2.84 ns and its weight fraction decreases to 59.4%. This suggests that most free carriers generated by illumination are efficiently transferred to the HTM, and that faster transfer occurs at the perovskite/PT interface than at that of perovskite/PEDOT:PSS, confirming the potential advantages of using thin-film PT instead of conventional PEDOT:PSS.

To gain deeper insight into the charge recombination kinetics, we studied the dependence of J_{sc} on light intensity (I) under different incident light intensities ranging from 0 to 100 $\text{mW}\cdot\text{cm}^{-2}$ (see Fig. 3(a)). J_{sc} is assumed to have a power-law dependence on I , using the equation $J_{sc} \propto I^\alpha$ (Eq. 1). The data are plotted on a log-log scale and fit to a power law in Fig. 3(a). For the device with the PT HTM, the fitting of the data yields $\alpha = 0.955$, close to 1, indicating that the charge collection efficiency is independent of light intensity.

This also may indicate sufficient electron and hole mobility with no substantial space charge build-up in the integrated device. Charge carrier losses in the absorber bulk may be dominated by monomolecular recombination via defects, while bimolecular recombination may cause only rather minor losses. [20] Electrochemical impedance spectroscopy (EIS) was employed to explain the significant difference in FF of the devices based on PT versus PEDOT:PSS. Similar impedance patterns for the perovskite solar cells as seen in previous reports [8, 21, 22] are presented in Fig. 4. The resistance of the conducting glass, contacts, and wires, R_S , can be determined from the intersection of the first arc at high frequency. The arc at high frequency is attributed to charge-transfer resistance (R_C) occurring at the interface and the interfacial capacitance between electrodes and HTM (or electron-transport material, ETM). The arc at intermediate frequency is ascribed to the charge-transport resistance (R_{HTM} or R_{ETM}) in the HTM or ETM, and these materials' corresponding capacitance, which decreases significantly regardless of illumination condition when bias is

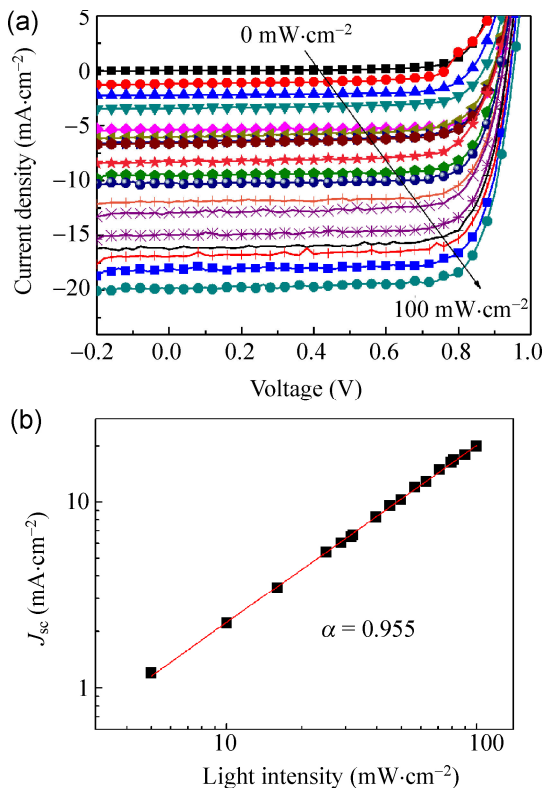


Figure 3 (a) J - V characteristics of PT/CH₃NH₃PbI₃/C₆₀ solar cells under various light intensities ranging from 100 to 0 $\text{mW}\cdot\text{cm}^{-2}$; (b) Measured J_{sc} plotted against light intensity on a logarithmic scale. Fitting a power law (eq 1) to these data yields α .

applied, indicates the reduction of their corresponding resistance. Furthermore, perovskite solar cells with PT as the HTM show lower resistance than those with PEDOT:PSS, possibly due to the lower resistance of PT compared to PEDOT:PSS. This decrease in R_{HTM} leads to a lower resistive voltage loss, which is a major factor in the observed increase in the FF for PT-based devices, consistent with previously published results. [8, 21, 22] Stability test results of HTM/CH₃NH₃PbI₃/C₆₀ perovskite solar cells are shown in Fig. S8, presenting the temporal evolution of the selected five-device performance for PT (or PEDOT:PSS)/CH₃NH₃PbI₃/C₆₀ perovskite cells. For PT/CH₃NH₃PbI₃/C₆₀ perovskite, the four key photovoltaic parameters of V_{oc} , J_{sc} , FF, and PCE increased to their highest value after 24 hours in a non-illuminated N₂ glove box. These parameters then exhibited excellent stability during exposure to illumination of simulated 100 $\text{mW}\cdot\text{cm}^{-2}$ AM 1.5 G irradiation in an N₂ glovebox with oxygen content of 30–70 ppm, water content of 0.01–0.1 ppm, and temperature of 25–35 °C over 816 hours. [14] However,

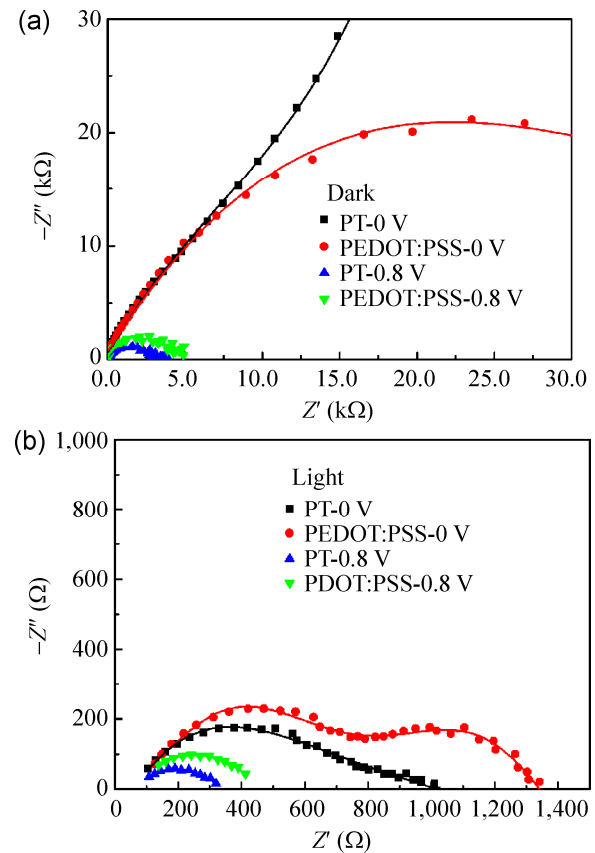


Figure 4 Nyquist plots of CH₃NH₃PbI₃ perovskite solar cells with PT and PEDOT:PSS as HTM, measured with frequency from 100,000 to 10 Hz at 0 V or 0.8 V bias (a) under no illumination; (b) under 100 $\text{mW}\cdot\text{cm}^{-2}$ illumination.

for the PEDOT:PSS/CH₃NH₃PbI₃/C₆₀ perovskite cell, the four key photovoltaic parameters drop sharply after one week of exposure, which may be due to the perovskite's damage by water absorbed by PEDOT:PSS.

In summary, we used ultrathin PT film prepared via electrochemical polymerization as a hole-transporting layer in a CH₃NH₃PbI₃ perovskite solar cell. Optimized devices with a 5-nm-thick PT film showed a promising power conversion efficiency of about 15.4%, a high FF of 0.774, good V_{oc} of 0.99 V, and J_{sc} of 20.3 $\text{mA}\cdot\text{cm}^{-2}$. The overall performance of the devices was superior to those using conventional PEDOT:PSS as the HTM. The high performance of these devices could originate from PT's energy levels matching the energy of CH₃NH₃PbI₃ perovskite's HOMO, PT's high hole conductivity, excellent wettability and compatibility with DMF, and faster charge transfer occurring between the PT and perovskite layers than between PEDOT:PSS and perovskite in the control cells. Furthermore, the

PT/CH₃NH₃PbI₃/C₆₀ perovskite solar cell showed high stability in a low-O₂-content and low-moisture atmosphere, due to PT's protection of CH₃NH₃PbI₃ perovskite from moisture. More importantly, using electrochemical polymerization to fabricate the ultrathin PT film is a simple, economic, and controllable method providing a feasible route to the large-scale production of HTM for perovskite solar cells.

Acknowledgements

The authors gratefully acknowledge the financial support from the National Basic Research Program (2011CB933303) and the National Natural Science Foundation of China (NSFC) (21321001, 21371012).

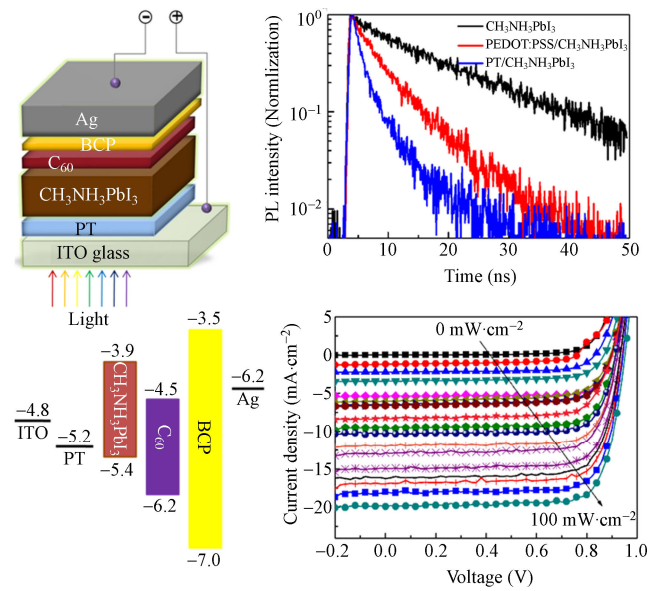
Electronic Supplementary Material: Supplementary material (experimental methods, preparation of materials, fabrication procedures of the device, and description of experimental setups) is available in the online version of this article at <http://dx.doi.org/10.1007/s12274-015-0755-5>.

References

- [1] Liu, D. Y.; Kelly, T. L. Perovskite solar cells with a planar heterojunction structure prepared using room-temperature solution processing techniques. *Nat. Photonics* **2014**, *8*, 133–138.
- [2] Wang, J. T. W.; Ball, J. M.; Barea, E. M.; Abate, A.; Alexander-Webber, J. A.; Huang, J.; Saliba, M.; Mora-Sero, I.; Bisquert, J.; Snaith, H. J. et al. Low-temperature processed electron collection layers of graphene/TiO₂ nanocomposites in thin film perovskite solar cells. *Nano Lett.* **2014**, *14*, 724–730.
- [3] Jeon, N. J.; Lee, H. G.; Kim, Y. C.; Seo, J.; Noh, J. H.; Lee, J.; Seok, S. I. O-methoxy substituents in spiro-OMeTAD for efficient inorganic-organic hybrid perovskite solar cells. *J. Am. Chem. Soc.* **2014**, *136*, 7837–7840.
- [4] Zhou, H. P.; Chen, Q.; Li, G.; Luo, S.; Song, T. B.; Duan, H. S.; Hong, Z. R.; You, J. B.; Liu, Y. S.; Yang, Y. Interface engineering of highly efficient perovskite solar cells. *Science* **2014**, *345*, 542–546.
- [5] Jeng, J. Y.; Chiang, Y. F.; Lee, M. H.; Peng, S. R.; Guo, T. F.; Chen, P.; Wen, T. C. CH₃NH₃PbI₃ perovskite/fullerene planar-heterojunction hybrid solar cells. *Adv. Mater.* **2013**, *25*, 3727–3732.
- [6] Pang, S. P.; Hu, H.; Zhang, J. L.; Lv, S. L.; Yu, Y. M.; Wei, F.; Qin, T. S.; Xu, H. X.; Liu, Z. H.; Cui, G. L. NH₂CH=NH₂PbI₃: An alternative organolead iodide perovskite sensitizer for mesoscopic solar cells. *Chem. Mater.* **2014**, *26*, 1485–1491.
- [7] Bi, D. Q.; Yang, L.; Boschloo, G.; Hagfeldt, A.; Johansson, E. M. J. Effect of different hole transport materials on recombination in CH₃NH₃PbI₃ perovskite-sensitized mesoscopic solar cells. *J. Phys. Chem. Lett.* **2013**, *4*, 1532–1536.
- [8] Christians, J. A.; Fung, R. C. M.; Kamat, P. V. An inorganic hole conductor for organo-lead halide perovskite solar cells. Improved hole conductivity with copper iodide. *J. Am. Chem. Soc.* **2014**, *136*, 758–764.
- [9] Wu, Z. W.; Bai, S.; Xiang, J.; Yuan, Z. C.; Yang, Y. G.; Cui, W.; Gao, X. Y.; Liu, Z.; Jin, Y. Z.; Sun, B. Q. Efficient planar heterojunction perovskite solar cells employing graphene oxide as hole conductor. *Nanoscale* **2014**, *6*, 10505–10510.
- [10] Yeo, J. S.; Kang, R.; Lee, S.; Jeon, Y. J.; Myoung, N.; Lee, C. L.; Kim, D. Y.; Yun, J. M.; Seo, Y. H.; Kim, S. S. et al. Highly efficient and stable planar perovskite solar cells with reduced graphene oxide nanosheets as electrode interlayer. *Nano Energy* **2015**, *12*, 96–104.
- [11] Bi, D. Q.; Moon, S. J.; Häggman, L.; Boschloo, G.; Yang, L.; Johansson, E. M. J.; Nazeeruddin, M. K.; Grätzel, M.; Hagfeldt, A. Using a two-step deposition technique to prepare perovskite (CH₃NH₃PbI₃) for thin film solar cells based on ZrO₂ and TiO₂ mesostructures. *RSC Adv.* **2013**, *3*, 18762–18766.
- [12] Min, J.; Zhang, Z. G.; Hou, Y.; Quiroz, C. O. R.; Przybilla, T.; Bronnbauer, C.; Guo, F.; Forberich, K.; Azimi, H.; Ameri, T. et al. Interface engineering of perovskite hybrid solar cells with solution-processed perylene-diimide heterojunctions toward high performance. *Chem. Mater.* **2015**, *27*, 227–234.
- [13] Azimi, H.; Ameri, T.; Zhang, H.; Hou, Y.; Quiroz, C. O. R.; Min, J.; Hu, M. Y.; Zhang, Z. G.; Przybilla, T.; Matt, G. J. et al. A universal interface layer based on an amine-functionalized fullerene derivative with dual functionality for efficient solution processed organic and perovskite solar cells. *Adv. Energy Mater.*, in press, DOI: 10.1002/aenm.201401692.
- [14] Haberreutinger, S. N.; Leijtens, T.; Eperon, G. E.; Stranks, S. D.; Nicholas, R. J.; Snaith, H. J. Carbon nanotube/polymer composites as a highly stable hole collection layer in perovskite solar cells. *Nano Lett.* **2014**, *14*, 5561–5568.
- [15] Heo, J. H.; Im, S. H.; Noh, J. H.; Mandal, T. N.; Lim, C.; Chang, J. A.; Lee, Y. H.; Kim, H.; Sarkar, A.; Nazeeruddin, M. K. et al. Efficient inorganic–organic hybrid heterojunction solar cells containing perovskite compound and polymeric hole conductors. *Nat. Photonics* **2013**, *7*, 486–491.

- [16] Jeon, N. J.; Lee, J.; Noh, J. H.; Nazeeruddin, M. K.; Grätzel, M.; Seok, S. I. Efficient inorganic–organic hybrid perovskite solar cells based on pyrene arylamine derivatives as hole-transporting materials. *J. Am. Chem. Soc.* **2013**, *135*, 19087–19090.
- [17] Zhou, H.; Hu X.; Lu, Y. FT-IR of copolymer film and multiple film of thiophene and 3-methylthiophene. *Chinese Journal of Light Scattering* **2004**, *15*, 311–315.
- [18] Yan, W. B.; Li, Y. L.; Sun, W. H.; Peng, H. T.; Ye, S. Y.; Liu, Z. W.; Bian, Z. Q.; Huang, C. H. High-performance hybrid perovskite solar cells with polythiophene as hole-transporting layer via electrochemical polymerization. *RSC Adv.* **2014**, *4*, 33039–33046.
- [19] Stranks, S. D.; Eperon, G. E.; Grancini, G.; Menelaou, C.; Alcocer, M. J. P.; Leijtens, T.; Herz, L. M.; Petrozza, A.; Snaith, H. J. Electron-hole diffusion lengths exceeding 1 micrometer in an organometal trihalide perovskite absorber. *Science* **2013**, *342*, 341–344.
- [20] Kyaw, A. K. K.; Wang, D. H.; Gupta, V.; Leong, W. L.; Ke, L.; Bazan, G. C.; Heeger, A. J. Intensity dependence of current-voltage characteristics and recombination in high-efficiency solution-processed small-molecule solar cells. *ACS Nano* **2013**, *7*, 4569–4577.
- [21] Kim, H. S.; Mora-Sero, I.; Gonzalez-Pedro, V.; Fabregat-Santiago, F.; Juarez-Perez, E. J.; Park, N. G.; Bisquert, J. Mechanism of carrier accumulation in perovskite thin-absorber solar cells. *Nat. Commun.* **2013**, *4*, 2242–2248.
- [22] Zheng, L. L.; Chung, Y. H.; Ma, Y. Z.; Zhang, L. P.; Xiao, L. X.; Chen, Z. J.; Wang, S. F.; Qu, B.; Gong, Q. H. A hydrophobic hole transporting oligothiophene for planar perovskite solar cells with improved stability. *Chem. Commun.* **2014**, *50*, 11196–11199.

Table of contents



Hybrid CH₃NH₃PbI₃ perovskite solar cells with ultrathin polythiophene as a hole-transporting layer show a low carrier recombination rate and fast hole-transfer, producing high-performance devices with excellent stability.

Electronic Supplementary Material

Stable high-performance hybrid perovskite solar cells with ultrathin polythiophene as hole-transporting layer

Weibo Yan¹, Yunlong Li¹, Yu Li², Senyun Ye¹, Zhiwei Liu¹, Shufeng Wang² (✉), Zuqiang Bian¹ (✉), Chunhui Huang¹ (✉)

¹ State Key Laboratory of Rare Earth Materials Chemistry and Applications, College of Chemistry and Molecular Engineering, Peking University, Beijing, 100871, China

² State Key Laboratory for Mesoscopic Physics, Department of Physics, Peking University, Beijing 100871, China

Supporting information to DOI 10.1007/s12274-015-0755-5

1. EXPERIMENTAL SECTION

Materials and methods: Thiophene and $\text{BF}_3\cdot\text{Et}_2\text{O}$ (BFEE) were purchased from J&K. PbI_2 , C_{60} , BCP, and Ag were purchased from Alfa Aesar and Sigma-Aldrich. Indium tin oxide (ITO)-coated glass substrates with sheet resistance of $24 \Omega/\text{sq}$ were purchased from CSG Holding Co., Ltd. $\text{BF}_3\cdot\text{Et}_2\text{O}$ was purified by distillation prior to its use. PdI_2 , C_{60} , and BCP were purified by vacuum sublimation. $\text{CH}_3\text{NH}_3\text{I}$ was synthesized according to literature procedures⁷ and recrystallized prior to use. Cyclic voltammograms were obtained in dichloromethane ($1\times 10^{-3} \text{ M}$) using tetrabutylammonium hexafluorophosphate (TBAPF₆) (0.1 M) as the supporting electrolyte at a scan rate of $0.1 \text{ V}\cdot\text{s}^{-1}$ and Fc/Fc⁺ as an internal reference during the measurement. The HOMO and LUMO energy levels were estimated relative to the energy level of a ferrocene reference (4.8 eV below vacuum level). UV-Vis spectra were obtained with a JASCO V-570 spectrophotometer. The IR spectrum of the PT was recorded by an ECTOR22 Fourier transform infrared spectrometer (FTIR). The work function of the PT film was measured by ultraviolet photoelectron spectroscopy (UPS) (Ac-2, Riken Keiki). The out-of-plane conductivity of the PT films was measured using a two-probe method with an Ag contact. XRD experiments were performed using a Rigaku D/max-2500 X-ray diffractometer with Cu-K α radiation at a generator voltage of 40 kV and a current of 100 mA. Atomic force microscope (AFM) investigation was performed using an SPA 400 in contact mode. Scanning electron microscope (SEM) investigation was performed with an SEM Hitachi S-4800 microscope. Film thicknesses were measured using a KLA-Tencor Alpha-Step IQ, TEM, and SEM. Impedance spectra were recorded at 0 V or 0.8 V bias with either no illumination or under $100 \text{ mW}\cdot\text{cm}^{-2}$ illumination, with frequency from 100,000 to 10 Hz, amplitude of 0.005 V, and quiet time of 2 s.

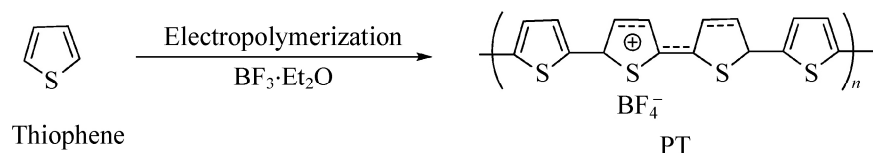
Address correspondence to Zuqiang Bian, email bianzq@pku.edu.cn; Shufeng Wang, email wangsf@pku.edu.cn

Synthesis of PT: PT films were synthesized in a one-compartment cell under computer control in a three-electrode test system according to references. [1, 2] The working electrode was ITO glass substrate (approximately $0.38 \times 2.2 \text{ cm}^2$) and the counter electrode was a platinum wire placed 0.5 cm away, while an Ag/AgCl electrode was used as the reference electrode. The electrolyte solution was freshly distilled BFEE containing 30 mM thiophene monomer for the synthesis of PT. All solutions were degassed with a stream of dry Ar and a slight overpressure was maintained during each experiment. The PT films were grown at +1.30 V in the optimized polymerization condition. The polymerization current was reduced from $1.00 \times 10^{-4} \text{ A}$ to $1.00 \times 10^{-5} \text{ A}$ and the reaction time was extended from 15 s to 200 s. After polymerization, the films were thoroughly rinsed with diethyl ether and ethanol, and then dried under flowing N₂.

Device fabrication and photovoltaic characterization: Solar cells were fabricated on pre-cleaned ITO-coated glass substrates. First, a thin (about 5 nm) PT layer was deposited on ITO-coated glass by electrochemical polymerization. Then the PT film was infiltrated with PbI₂ by spin-coating at 8,000 rpm for 60 s with a PbI₂ solution in dimethylformamide (DMF) (462 mg·mL⁻¹, at 20 °C) in a N₂ glove box. After drying, the film was dipped in a CH₃NH₃I solution in 2-propanol (10 mg·mL⁻¹) at 70 °C for 90 s in air, then rinsed with 2-propanol. After the CH₃NH₃I perovskite was annealed at 100 °C for 40 min in air, C₆₀ (30–50 nm)/BCP (5–15 nm) were deposited sequentially under high vacuum. Finally, Ag (100 nm) was thermally evaporated on top of the device to form the cell's back contact.

The current density-voltage (*J-V*) curves of the photovoltaic devices were obtained by a Keithley 4200 source-measure unit with a scanning forward direction from -0.3 to 1.3 V and reverse direction from 1.3 to -0.3 V with a sweep rate of 0.3 V·s⁻¹. The photocurrent was measured under simulated 100 mW·cm⁻² AM 1.5 G irradiation using a Xe-lamp-based solar simulator [Oriel 300 W solar simulator (Thermo Oriel 91160–1000)] in a N₂ glove box with pressure of 0.02 mbar, O₂ content of 40–70 ppm, and water content of 0.005–0.01 ppm. The simulated irradiance was calibrated using a certified silicon diode, as determined by a standard silicon solar cell. The effective area of the cell was defined as approximately 0.10 cm² using a non-reflective photo mask. The IPCE was recorded on Keithley 2400 source meter under irradiation by a 150 W tungsten lamp with a 0.25 m monochromator (Spectral Product DK240).

2. CHARACTERIZATION SECTION



Scheme S1 Synthetic route for PT by electrochemical polymerization at 1.3 V under Ar atmosphere.

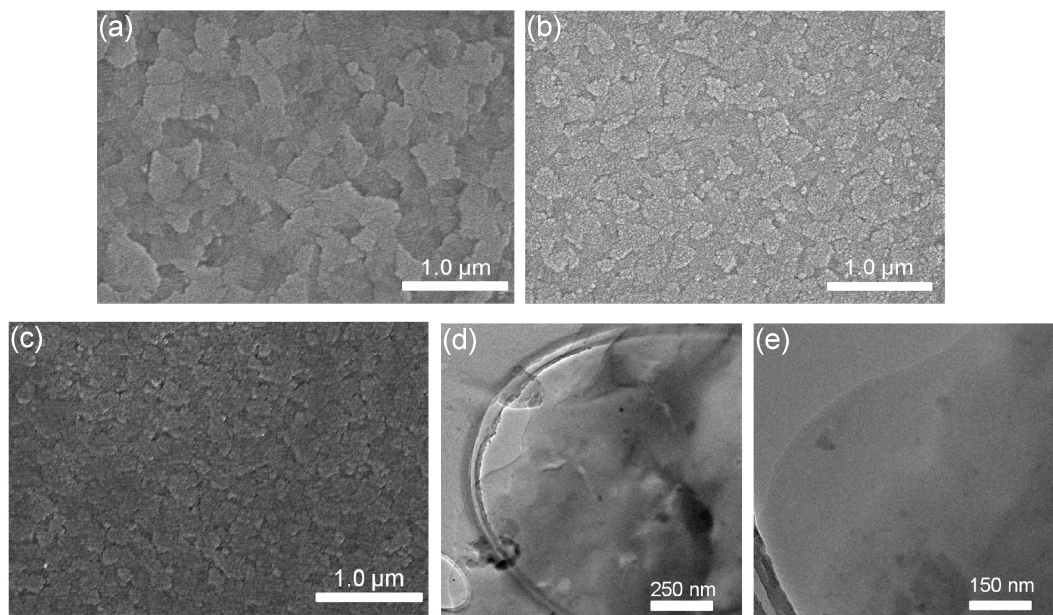


Figure S1 SEM micrograph of the surface of (a) ITO substrate; (b) the PT film prepared by previous method; (c) the PT film prepared by modified method. TEM of PT film peeled from ITO/glass (d) by previous method; (e) by present modified method.

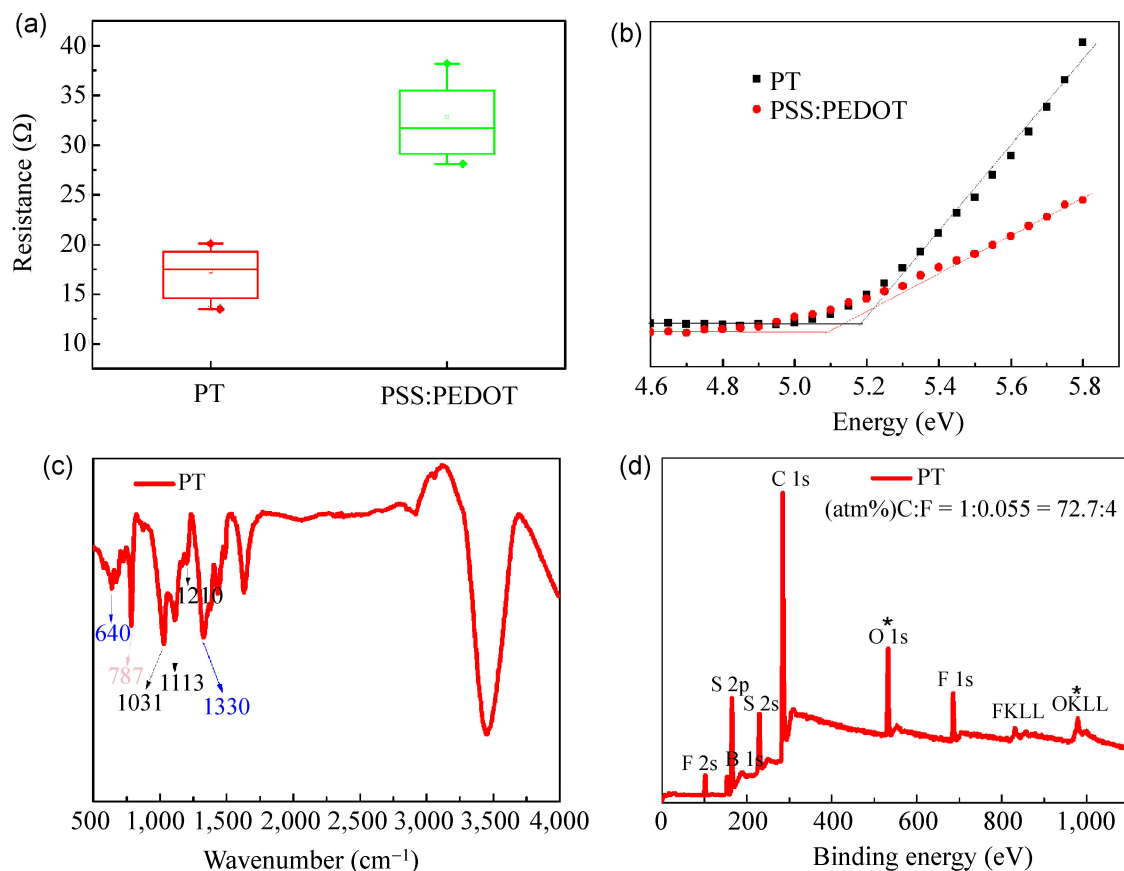


Figure S2 (a) The conductivity of the PT or PEDOT:PSS HTM layer; (b) UPS spectrum of the PT or PEDOT:PSS film; (c) FTIR spectrum of PT; (d) XPS spectrum of PT.

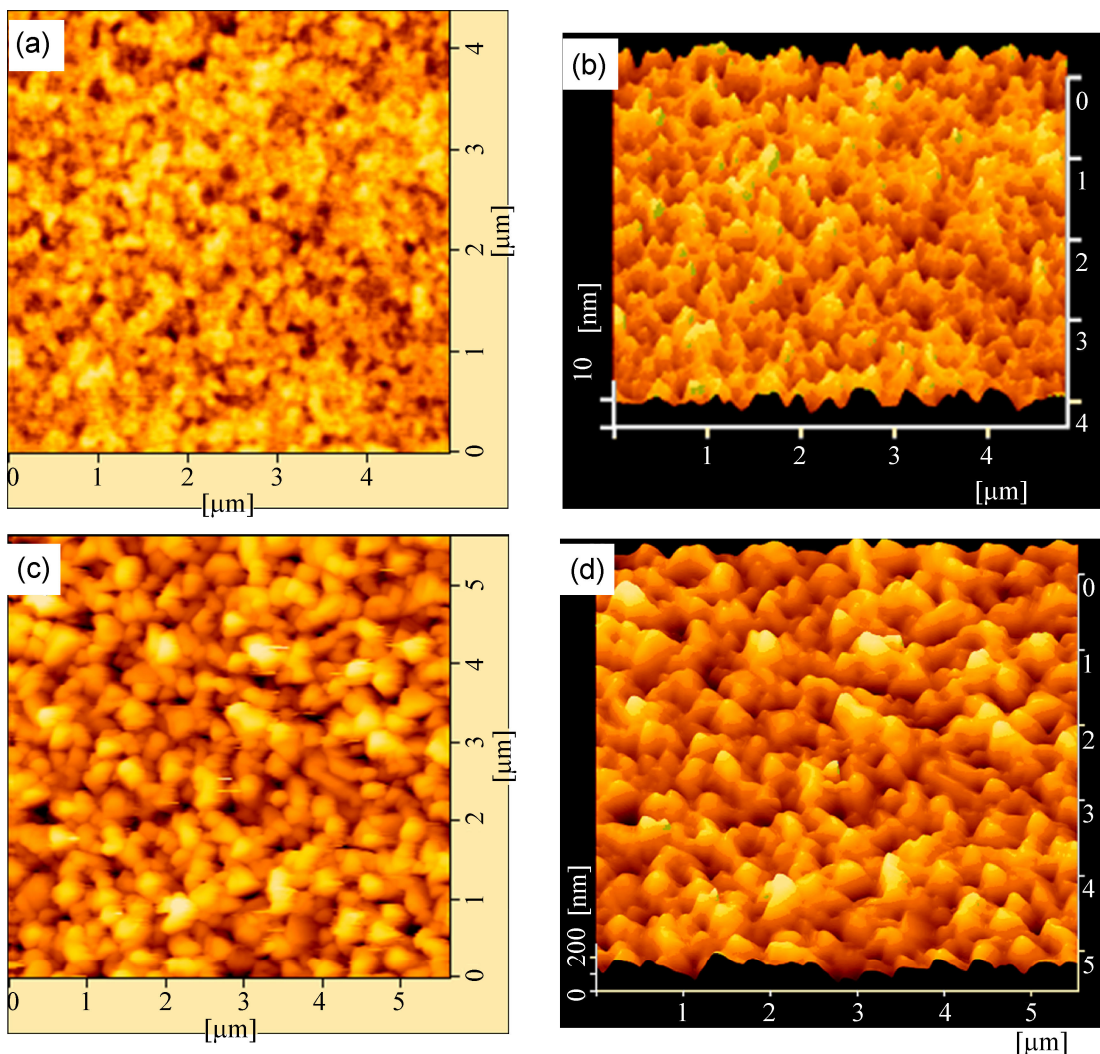


Figure S3 AFM of the surface of (a) the PT film on ITO glass substrate; (b) 3D pattern of the PT film with RMS = 2.3 nm; (c) the $\text{CH}_3\text{NH}_3\text{PbI}_3$ film on PT/ITO glass substrate; (d) 3D pattern of the $\text{CH}_3\text{NH}_3\text{PbI}_3$ film with RMS = 31.5 nm.

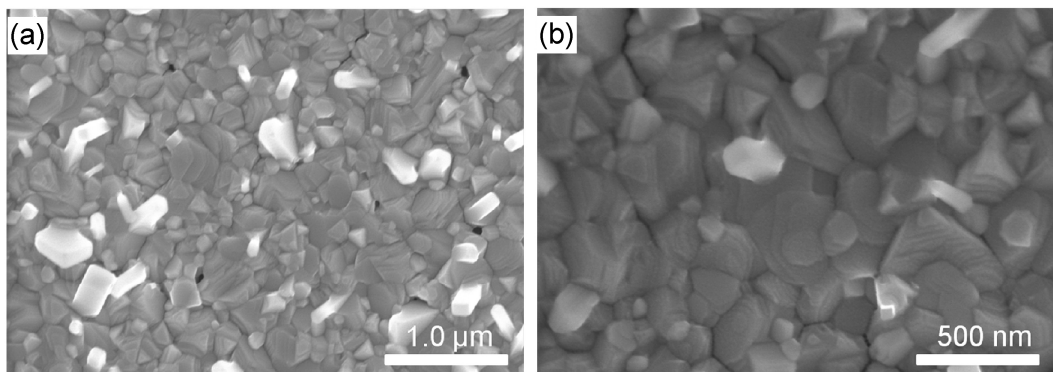


Figure S4 SEM micrographs of the surface of the $\text{CH}_3\text{NH}_3\text{PbI}_3$ film on the PT/ITO glass substrate (a) Low-magnification micrograph; (b) High-magnification micrograph.

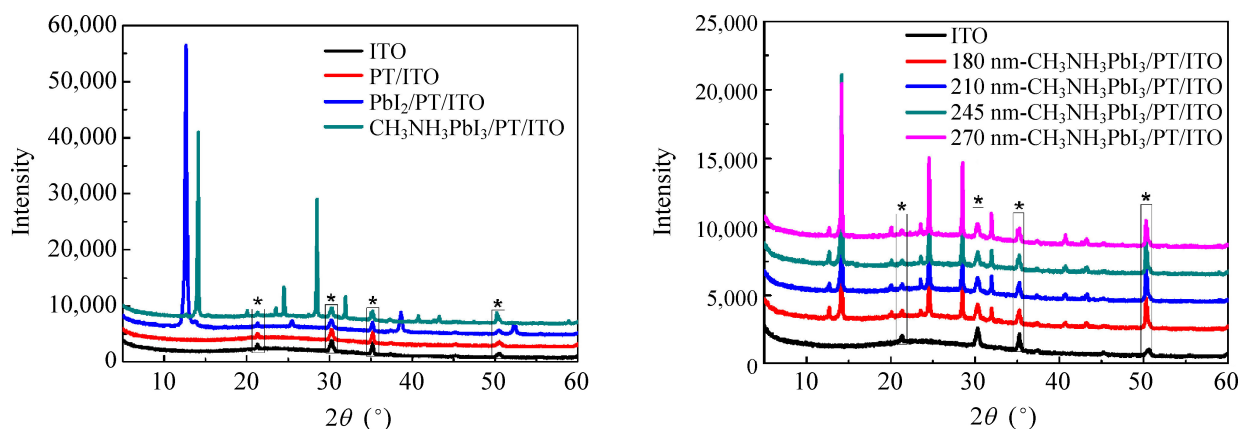


Figure S5 (a) GAXRD patterns of the PbI₂/glass, ITO substrate, ITO/PT, and CH₃NH₃PbI₃/PT/ITO/glass samples; (b) GAXRD patterns of the CH₃NH₃PbI₃/PT/ITO/glass samples with different thicknesses.

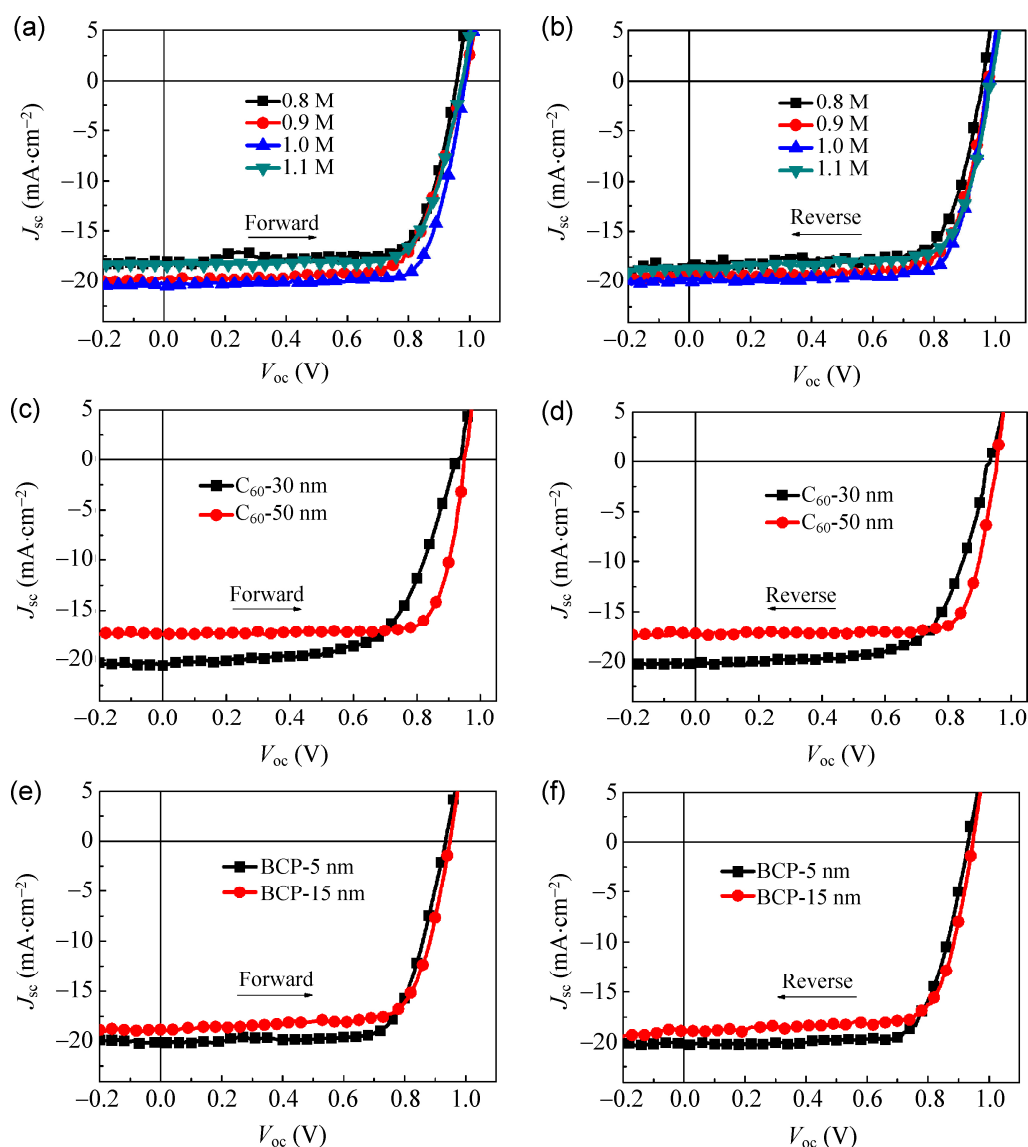


Figure S6 Current-density/voltage curves of the best-performing planar-heterojunction HTM/perovskite/C₆₀ solar cells with different concentrations of PbI₂ solution (0.8, 0.9, 1.0, and 1.1 M) by (a) forward or (b) reverse scan; different thickness of C₆₀ films (30 and 50 nm) by (c) forward or (d) reverse scan; different thickness of BCP films (5 and 15 nm) by (e) forward or (f) reverse scan.

Table S1 Device parameters of solar cells prepared by varying the layer thickness of $\text{CH}_3\text{NH}_3\text{PbI}_3$ perovskite with C_{60} (40 nm) and BCP (10 nm) under AM 1.5 G Illumination ($100 \text{ mW}\cdot\text{cm}^{-2}$)

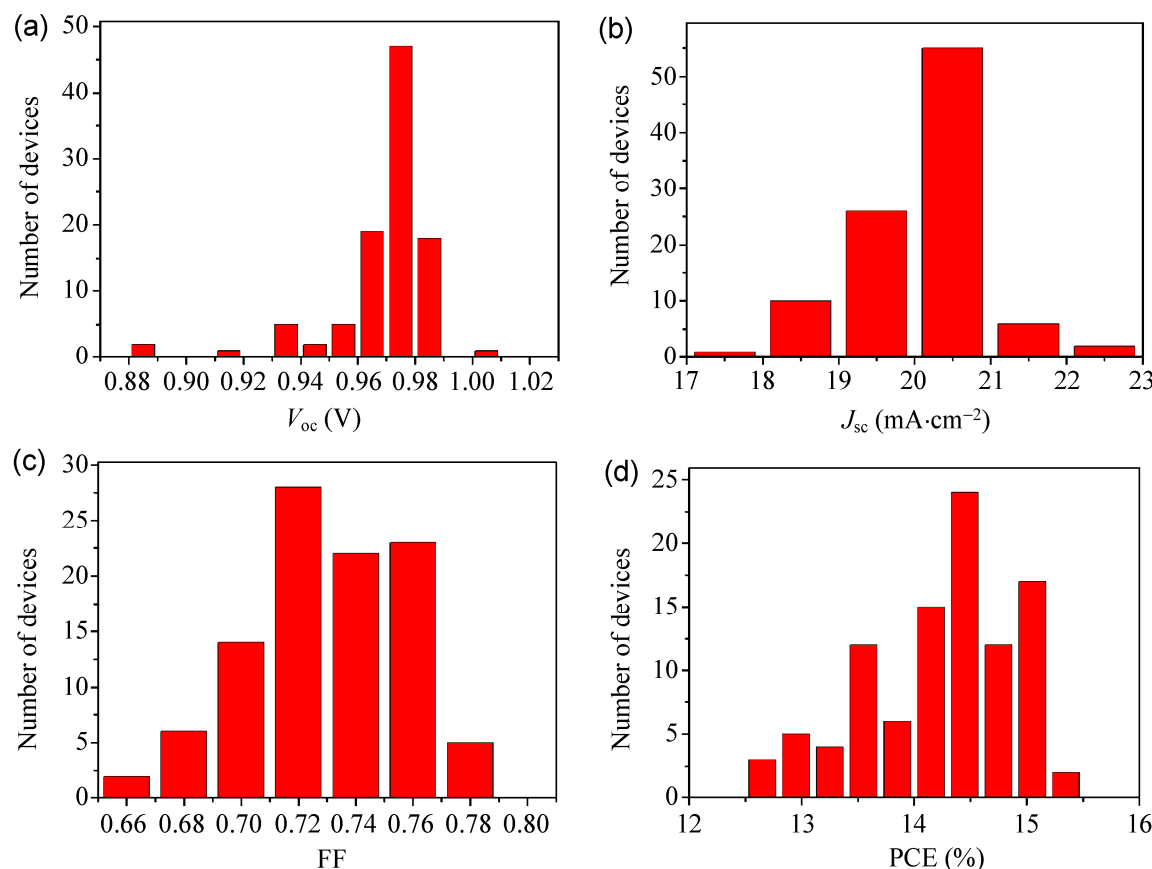
| PbI ₂ concentration (M) | Perovskite thickness (nm) | V_{oc} (V) | J_{sc} ($\text{mA}\cdot\text{cm}^{-2}$) | FF (%) | PCE (%) |
|------------------------------------|---------------------------|---------------------|---|---------------------|---------------------|
| 0.8 | 178 (± 4) | 0.96 (± 0.02) | 18.1 (± 0.7) | 0.72 (± 0.02) | 12.8 (± 0.07) |
| 0.9 | 210 (± 4) | 0.95 (± 0.02) | 19.6 (± 0.5) | 0.73 (± 0.02) | 13.7 (± 0.08) |
| 1.0 | 245 (± 10) | 0.97 (± 0.03) | 20.2 (± 1.0) | 0.75 (± 0.04) | 14.7 (± 0.70) |
| 1.1 | 270 (± 10) | 0.96 (± 0.03) | 18.7 (± 0.9) | 0.74 (± 0.04) | 13.4 (± 0.70) |

Table S2 Device parameters of solar cells prepared by varying the layer thickness of C_{60} with $\text{CH}_3\text{NH}_3\text{PbI}_3$ perovskite (245 nm) and BCP (10 nm) under AM 1.5 G Illumination ($100 \text{ mW}\cdot\text{cm}^{-2}$)

| C_{60} thickness (nm) | V_{oc} (V) | J_{sc} ($\text{mA}\cdot\text{cm}^{-2}$) | FF (%) | PCE (%) |
|--------------------------------|---------------------|---|---------------------|---------------------|
| 30 | 0.92 (± 0.03) | 20.3 (± 0.8) | 0.63 (± 0.08) | 12.5 (± 1.00) |
| 40 | 0.97 (± 0.03) | 20.2 (± 1.0) | 0.75 (± 0.04) | 14.7 (± 0.70) |
| 50 | 0.93 (± 0.04) | 17.4 (± 1.0) | 0.78 (± 0.03) | 12.2 (± 1.00) |

Table S3 Device parameters of solar cells prepared by varying the layer thickness of BCP with $\text{CH}_3\text{NH}_3\text{PbI}_3$ perovskite (245 nm) and C_{60} (40 nm) under AM 1.5G Illumination ($100 \text{ mW}\cdot\text{cm}^{-2}$)

| BCP thickness (nm) | V_{oc} (V) | J_{sc} ($\text{mA}\cdot\text{cm}^{-2}$) | FF (%) | PCE (%) |
|--------------------|---------------------|---|---------------------|---------------------|
| 5 | 0.94 (± 0.02) | 19.9 (± 1.0) | 0.73 (± 0.03) | 13.6 (± 1.00) |
| 10 | 0.97 (± 0.03) | 20.2 (± 1.0) | 0.75 (± 0.04) | 14.7 (± 0.70) |
| 15 | 0.93 (± 0.04) | 18.6 (± 0.8) | 0.72 (± 0.04) | 12.7 (± 1.00) |

**Figure S7** (a)–(d) Histograms of device parameters measured for 100 separate ITO/PT(5 nm)/ $\text{CH}_3\text{NH}_3\text{PbI}_3$ (245 nm)/ C_{60} (40 nm)/BCP(10 nm)/Ag(100 nm) devices. (a) V_{oc} , (b) J_{sc} , (c) FF, and (d) PCE.

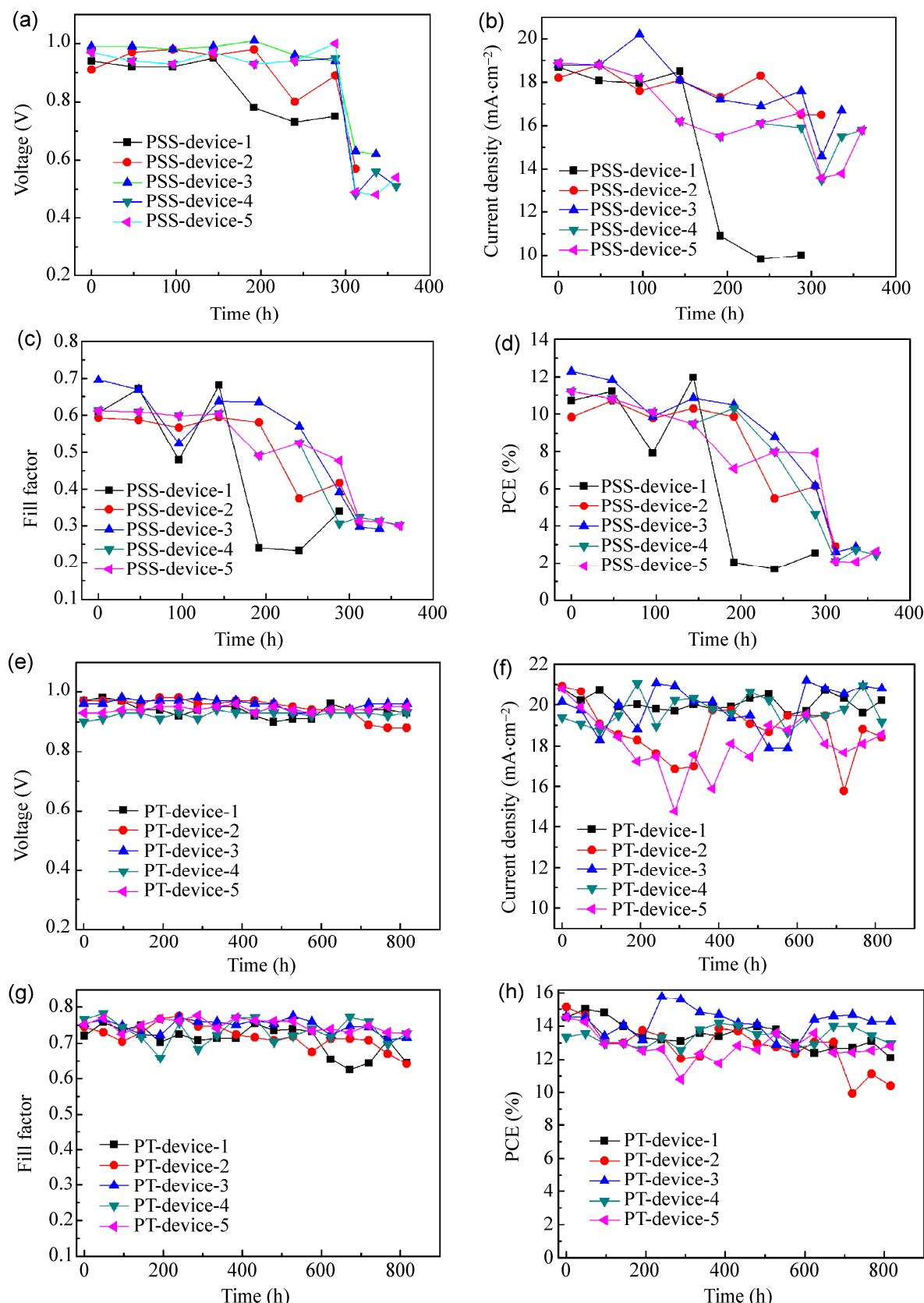


Figure S8 Stability test of five PT (or PEDOT:PSS)/ $\text{CH}_3\text{NH}_3\text{PbI}_3/\text{C}_{60}$ perovskite solar cell devices, performed under simulated $100 \text{ mW} \cdot \text{cm}^{-2}$ AM 1.5 G irradiation in N_2 glovebox with O_2 content of about 60 ppm, water content of 0.01 ppm and temperature of 25–35 °C over 816 h.

Time-resolved photoluminescence measurements

The femtosecond time-resolved fluorescence spectra were recorded by a high-resolution streak camera system (Hamamatsu C10910). An amplified mode-lock Ti:sapphire laser system (Legend, Coherent) delivered a pulse of 800 nm and 35 fs with repetition of 1 KHz. The laser beam was used to pump a two-stage optical parametric amplifier (OperA Solo, Coherent) to generate the pump beam. All samples were excited by 517 nm radiation at room temperature with 135 nJ cm⁻²/pulse. The lifetime was obtained by fitting the PL spectra measured from the perovskite films with a bi-exponential decay function of the form: [3]

$$I(t) = A_1 \exp\left(-\frac{t}{\tau_1}\right) + A_2 \exp\left(-\frac{t}{\tau_2}\right)$$

Table S4 Time-resolved photoluminescence characterization of the two-step prepared CH₃NH₃PbI₃ perovskite. Data were collected at the maximum CH₃NH₃PbI₃ perovskite emission (770 nm)

| Substrate | HTM | τ_1 (ns) | Fraction | τ_2 (ns) | Fraction |
|-----------|-----------|---------------|----------|---------------|----------|
| ITO | non | 3.60 | 23.6% | 17.3 | 76.4% |
| ITO | PEDOT:PSS | 2.84 | 59.4% | 7.69 | 40.6% |
| ITO | PT | 1.17 | 83.2% | 4.81 | 16.8% |

References

- [S1] Yan, W.; Li, Y.; Sun, W.; Peng, H.; Ye, S.; Liu, Z.; Bian, Z.; Huang, C. High-performance hybrid perovskite solar cells with polythiophene as hole-transporting layer via electrochemical polymerization. *RSC Adv.* **2014**, *4*, 33039–33046.
- [S2] Jin, S.; Cong, S.; Xue, G.; Xiong, H.; Mansdorf, B.; Chen, S. Z. D. Anisotropic polythiophene films with high conductivity and good mechanical properties via a new electrochemical synthesis. *Adv. Mater.* **2002**, *14*, 1492–1496.
- [S3] Liang, P.; Liao, C.; Chueh, C.; Zuo, F.; Williams, S. T.; Xin, X.; Lin, J.; Jen, A. K.-Y. Additive enhanced crystallization of solution-processed perovskite for highly efficient planar-heterojunction solar cells *Adv. Mater.* **2014**, *26*, 3748–3754.